50th AIAA/ASME/ASCE/AHS/ASC Structures, Structural Dynamics, and Materials Conference
17th
4 - 7 May 2009, Palm Springs, California

AIAA 2009-2684

Elastic Properties of Foams with Tetrakaidecahedral Cells Using Finite Element Analysis

Prasanna Thiyagasundaram[1] Bhavani V. Sankar[2] Nagaraj K.Arakere[3]
University of Florida, Gainesville, Florida, 32611-6250

A finite element method based micromechanics has been used for predicting the orthotropic properties of foams which have tetrakaidecahedral unit-cells. Both equi-sided and Kelvin-elongated tetrakaidecahedrons are studied. The results for elastic constants from the FE models agree well with that of available analytical models. The struts were modeled using both Euler-Bernoulli and Timoshenko beam elements. It is found that classical beam theory over predicts the elastic moduli when the struts have smaller length to thickness ratio.

Nomenclature

a_1	=	Length of the representative volume element
a_2	=	Width of the representative volume element
a_3	=	Height of the representative volume element
V	=	Volume of the representative volume element
f_{ij}	=	Force in the direction i when displacement is applied in the direction j
$\Delta_1, \Delta_2, \Delta_3$	=	Components of an arbitrary displacement vector Δ in the principal X, Y, and Z directions
U	=	Strain energy of the system
$\varepsilon_1, \varepsilon_2, \varepsilon_3$	=	Strain components in the principal X, Y, and Z directions
U_0	=	Strain energy density of the system
$[C]$	=	Stiffness matrix of the foam
ε_{ij}	=	Macro-strain
u_i	=	Displacement in the i direction
ε_0	=	Applied macro-strain
E_i	=	Young's modulus along axis i
G_{ij}	=	Shear modulus in direction j on the plane whose normal is in direction i
v_{ij}	=	Poisson's ratio
I_x, I_y	=	Moment of inertia in the X and the Y directions
J	=	Polar moment of inertia
ρ_s	=	Density of the strut material
E_s	=	Elastic modulus of the strut material
v_s	=	Poisson's ratio of the strut material
A	=	Cross sectional area
D	=	Length of the side of the equilateral triangle cross section
l	=	Length of each individual edge of the equisided tetrakaidecahedron
r	=	Radius of the 3-cusp hypocycloid cross section
ΔU_i	=	Difference in translational displacement along axis i
$\Delta\theta_i$	=	Difference in rotational displacement along axis i

[1]Graduate Student & Corresponding Author, Department of Mechanical Engineering, 127 NEB, PO Box 116250, University of Florida (pthiyaga@ufl.edu)
[2]Newton C. Ebaugh Professor, Department of Mechanical Engineering, University of Florida, Associate Fellow AIAA. (sankar@ufl.edu)
[3]Associate Professor, Department of Mechanical and Aerospace Engineering, University of Florida (nagaraj@ufl.edu)

I. Introduction

Cellular solids are special materials made out of solid strut or thin plate like structures bridged together[1].They occur in nature in the form of honeycombs, wood, bone, cork etc. These materials exploit a unique combination of properties such as high thermal resistance, low density and high energy-absorption. Foams are a class of cellular solids, generally made by dispersing gas into a liquid material and then cooling it to solidify. They are categorized as open-cell and closed-cell foams. Depending on the solid materials that are made into foams, they are also categorized as polymeric foams, metallic foams, and ceramic foams[1]. Due to developments in material science and manufacturing techniques, advanced foams have found a great potential for use in automobile, aircraft, and space vehicle structures. A special example is the use of foams in external fuel tanks and thermal protection system (TPS) in space vehicles. It has been accepted that packed in a BCC structure, a tetrakaidecahedron – a 14-faced polyhedron - satisfies the minimum surface energy condition for mono-dispersed bubbles[2]. These tetrakaidecahedral foams have held the interest of researchers for decades. Microcellular graphitic carbon foams were first developed at the US Air Force Research Laboratory in the 1990s[3]. Clearly, it has been proven that the repeating unit cell of this foam can be approximated by a regular tetrakaidecahedron[4].

The catastrophic failure of Space Shuttle Columbia in February 2003 has given the necessary impetus to understand and reduce the likelihood and severity of foam shedding events that occur from the Shuttle's external fuel tanks. Currently, there is lot of ongoing research focused on understanding the mechanisms that cause foam fracture and debris liberation[5]. This mandates a thorough understanding of the foam's mechanical response behavior in the form of characterization of its elastic properties.

In the same context, a lot of work in the field of aerostructural composites has taken place in characterizing materials using the principles of micromechanics[6,7]. These principles that call upon simulating a characteristic representative part of the structure that periodically repeats itself, instead of simulating the entire model has effectively been used in foams[8]. Foams with simple representative unit cell structures such as cube[8], to hexagonal cell structures[1], to a regular tetrakaidecahedron[9] as the unit cell, have been carefully studied and characterized for their mechanical behavior.

Currently, BX-265 and NCFI24-124 are the 2 foams used most exclusively in space shuttle external tanks. The photomicrographs[10] of these 2 foams are shown in Figure 1 and Figure 2. Analysis of the foam structure from these micrographs has shown that due to forming and rising process that takes place during fabrication, the unit cell of these foam structures is elongated in one of the three principal directions. Hence, this unit cell is called an elongated tetrakaidecahedron and the elongated direction is referred to as the 'rise direction' (Figure 3). This kind of structure makes the foam anisotropic.

Broadly, the available literature on foam mechanics can be classified into understanding foams from experimental observations[10, 12, 13] or understanding foams by developing appropriate analytical models[11, 14].

Analytical models that have been developed focus primarily on predicting the mechanical and strength properties. Assuming that the unit cell edges behave like a three dimensional beam, the mechanics of deformation of the elongated tetrakaidecahedron leads to a set of equations for the effective Young's modulus, Poisson's ratio and tensile strength of the foam in the principal material directions[10]. The equations for these elastic constants have been derived and written in terms of the cell edge length, and the axial, flexural and torsional rigidities of the strut cross section. Also the variation of these properties with 'relative density' (the ratio of the density of the cellular medium to the density of the solid strut material) of the foam has been expressed.

The current paper explores the possibility of using finite element based micromechanics procedures to calculate the elastic properties of foam materials and to extend this procedure for developing multi-axial failure envelopes. In order to do this, boundary conditions in the form of periodic boundary conditions have been derived and have been applied to the unit cell model. The results obtained from this method have been compared with the results obtained from existing analytical models[10] and they have been shown to match well for some of the elastic constants. Also, the advantages of using finite element based methods over analytical methods have been highlighted.

II. Finite Element Modeling of a Tetrakaidecahedron Unit Cell

The most general geometry of a tetrakaidecahedron has 24 vertices and 36 edges comprising of 8 hexagons and 6 quadrilaterals (Figure 3). It is more precisely called truncated octahedron, since it is created by truncating the corners of an octahedron[15]. A regular tetrakaidecahedron is generated by truncating the corners of a cube[14]. This is called an equi-sided tetrakaidecahedron. If it is generated by truncating the corners of a cuboid or hexahedron, it is called an elongated tetrakaidecahedron[10].

An equi-sided tetrakaidecahedron has all edges of equal length. In this study, the commercially available ABAQUS® finite element software is employed for developing the model. A model for the equi-sided tetrakaidecahedron is shown in Figure 3. The principal directions *X*, *Y*, and *Z* are considered to be along the lines passing through the centers of the squares (Figure 3) on the front and back, the left and right and the top and the bottom, respectively. Including the squares and the hexagons in the unit cell model, the tetrakaidecahedron unit cell is made up of 24 beam elements.

The geometry and the material properties of the constituent strut material used in the equi-sided tetrakaidecahedron model are listed in Table 1. The strut material is considered as isotropic. In the current example the beam cross sections are considered to be equilateral triangles. The beam cross-sections are oriented such that the bisector of one of the angles of the triangular cross section at the center of the strut passes through the unit-cell center. The orientation of the cross section for one of the edges is shown in Figure 5. The section properties used in the model are listed in Table 2. Similar to an equisided tetrakaidecahedron, the geometry of an elongated tetrakaidecahedron is shown in Figure 6. The properties of the same are shown in Table 3.

The use of beam elements to model the struts needs some explanation. Strictly the beam model will be valid only if the struts are slender and behave like a beam. This requires a slenderness ratio (L/r, where L is the length of the strut, r is the radius of gyration defined by $r^2=I/A$) greater than about 10. If the slenderness ratio is less than 10 but greater than, say, 6, one can use shear-deformable beam elements and hope to obtain good results. If r is less than 6, one cannot use beam elements to model the deformation of the struts. One needs to resort to solid elements

For both equi-sided and elongated tetrakaidecahedron, two-node beam elements (classical Euler-Bernoulli beam element, B33 in the ABAQUS® material library) with cubic formulation were used to model the unit cell. Then, in order to get a comparison with the results of 2-node cubic elements, 3-node quadratic elements (shear deformable Timoshenko beam elements, B32 in the ABAQUS® material library) were used to model. The FE mesh is shown in Figure 7.

III. Periodic Boundary Conditions

For computing the elastic constants using micromechanics, we need equations that relate the micro-strains to the corresponding macro-strains. Using these equations, the periodic boundary conditions can be derived. From the periodicity of the cell structure (Figure 8), the representative volume element is identified to be the smallest cuboid that completely encloses the tetrakaidecahedron such that 6 square sides of the tetrakaidecahedron are on the 6 faces of the cuboid.

In this section we derive the periodic boundary conditions that will be used to derive the elasticity matrix of the idealized foam. Consider the deformation gradient $\varepsilon_{ij} = u_{i,j}$ at macro-scale. We would like to subject the RVE to a deformation such that the average of the above deformation gradient is equal to $\bar{\varepsilon}_{ij}$. Then this condition can be represented as

$$\bar{\varepsilon}_{ij} = \frac{1}{V}\int_V \frac{\partial u_i}{\partial x_j} dV \tag{1}$$

where V is the RVE volume. By applying divergence theorem to the right hand side of the above equation, the volume integral is converted into surface integral as

$$\bar{\varepsilon}_{ij} = \frac{1}{V}\int_S u_i n_j dS \tag{2}$$

where the integration is performed over the surface of the cuboid. Noting that n_j is non-zero only on two surfaces that are normal to the j direction, the above equation can be written as

$$\bar{\varepsilon}_{ij} = \frac{1}{V}\left(u_i^{+j} - u_i^{-j}\right) A_j \tag{3}$$

where A_j is the area of the face normal to j-direction, $u_i^+ - u_i^-$ represent the difference in the displacements u_i on the two surfaces normal to the j-direction. The superscripts $+j$ and $-j$ indicate, respectively, the two surfaces with positive and negative normals in the j-direction. From the above equation we obtain the periodic boundary condition as

$$u_i^{+j} - u_i^{-j} = \bar{\varepsilon}_{ij}\frac{V}{A_j} = \bar{\varepsilon}_{ij} a_j \tag{4}$$

Then the periodic BC for the three normal strains can be written as

$$u_i^{+i} - u_i^{-i} = \bar{\varepsilon}_{ii} a_i \quad (i=1,2,3;\ \text{no summation over } i) \tag{5}$$

For the case of shear strains the periodic BCs are not unique as the shear strain is given by the sum of two deformation gradients, $\gamma_{ij} = u_{i,j} + u_{j,i}$. Thus, one can apply either deformation gradient alone or both together. If, for example, one applies only $u_{i,j}$, then the BCs take the form

$$u_i^{+j} - u_i^{-j} = \bar{\gamma}_{ij} a_j; \qquad u_j^{+i} - u_j^{-i} = 0 \tag{6}$$

On the other hand if one chooses $u_{i,j} = u_{j,i} = \frac{\gamma_{ij}}{2}$, then two sets of BCs have to be applied as shown below:

$$u_i^{+j} - u_i^{-j} = \frac{\bar{\gamma}_{ij} a_j}{2}; \qquad u_j^{+i} - u_j^{-i} = \frac{\bar{\gamma}_{ij} a_i}{2} \tag{7}$$

The above periodic BCs are explicitly presented in Tables 5a through 5c. Table-5a, Table-5b, Table-5c shows the periodic boundary conditions in the form of difference in displacements between the set of nodes for the 3 unit strain load cases in the three principal directions. Figure 9, Figure 10 and Figure 11 show the pairs of node numbers that are subjected to these periodic boundary conditions. By using the forces that result after the unit strains are applied, the stiffness matrix for the foam can be computed.

IV. Derivation of the Elastic Constants

In this section we derive the procedures for determining the equivalent elastic constants of the tetrakaidechahedral foam idealized as an orthotropic material. The representative volume element (RVE) of the foam is a cuboid. The equivalent orthotropic material has its principal material directions parallel to the edges of the cuboid. In this coordinate system the normal and shear deformations are uncoupled. First we will derive the equations to determine the Young's moduli and Poisson's ratios in the principal material coordinates, 1, 2 and 3. The stress strain relations are written as:

$$\begin{Bmatrix} \sigma_1 \\ \sigma_2 \\ \sigma_3 \end{Bmatrix} = \begin{bmatrix} C_{11} & C_{12} & C_{13} \\ C_{21} & C_{22} & C_{23} \\ C_{31} & C_{32} & C_{33} \end{bmatrix} \begin{Bmatrix} \varepsilon_1 \\ \varepsilon_2 \\ \varepsilon_3 \end{Bmatrix} \tag{1}$$

We subject the RVE to three independent deformations such that in each case only one normal strain is non-zero and other two normal strains are equal to zero. For example, in the first case we apply periodic boundary conditions such that the cuboid expands only in the 1-direction and the strains in the other two directions are equal to zero, i.e., the dimensions of the cuboid in those directions do not change. Let the relative displacement between the two surfaces normal to the 1-direction be $\Delta_1=a_1$ such that $\varepsilon_1=1$. Corresponding force resultants in the three faces are F_{11}, F_{21} and F_{31} (see Figure 13). Similarly we can deform the RVE in the other directions and calculate the force resultants on each face. The forces can be written as a matrix

$$F = \begin{bmatrix} F_{11} & F_{12} & F_{13} \\ F_{21} & F_{22} & F_{23} \\ F_{31} & F_{32} & F_{33} \end{bmatrix} \tag{2}$$

Where F_{ij} will correspond to resultant or total forces on a face normal to the i^{th} direction when the only non-zero normal strain is $\varepsilon_j=1$.

Instead of applying unit normal strains, if we deform the RVE by applying unit displacements, then the forces will be different. The forces will scale with the length of the cuboid and we define a new matrix [*f*] which is similar to [*F*], but defines the forces for unit –displacements. The matrix [*f*] can be derived as

$$\begin{aligned} [f] &= \begin{bmatrix} F_{11}/a_1 & F_{12}/a_2 & F_{13}/a_3 \\ F_{21}/a_1 & F_{22}/a_2 & F_{23}/a_3 \\ F_{31}/a_1 & F_{32}/a_2 & F_{33}/a_3 \end{bmatrix} \\ &= [F]*[a]^{-1} \end{aligned} \tag{3}$$

Where [*a*] is given by the diagonal matrix

$$[a] = \begin{bmatrix} a_1 & 0 & 0 \\ 0 & a_2 & 0 \\ 0 & 0 & a_3 \end{bmatrix}$$

Let us assume the cuboid is subjected to an arbitrary deformation such the elongations parallel to the three directions are, respectively, Δ_1, Δ_2 and Δ_3. Then, the corresponding forces $\{f_\Delta\}$ to produce such a deformation could be easily computed as

$$\{f_\Delta\} = [f][\Delta]$$

The strain energy in the RVE due to such deformation is given by

$$\begin{aligned} U &= \frac{1}{2}[\Delta_1 \quad \Delta_2 \quad \Delta_3][f_\Delta] \\ &= \frac{1}{2}[\Delta_1 \quad \Delta_2 \quad \Delta_3][f]\begin{Bmatrix}\Delta_1\\ \Delta_2\\ \Delta_3\end{Bmatrix} \end{aligned} \tag{4}$$

The displacements Δ_1, Δ_2 and Δ_3 in the above strain energy expression can be expressed in terms of strains such that

$$\begin{aligned} U &= \frac{1}{2}[\varepsilon_1 a_1 \quad \varepsilon_2 a_2 \quad \varepsilon_3 a_3][f]\begin{Bmatrix}\varepsilon_1 a_1\\ \varepsilon_2 a_2\\ \varepsilon_3 a_3\end{Bmatrix} \\ &= \frac{1}{2}\ \varepsilon_1 \quad \varepsilon_2 \quad \varepsilon_3 \begin{bmatrix} a_1 & 0 & 0\\ 0 & a_2 & 0\\ 0 & 0 & a_3\end{bmatrix}[f]\begin{bmatrix} a_1 & 0 & 0\\ 0 & a_2 & 0\\ 0 & 0 & a_3\end{bmatrix}\begin{Bmatrix}\varepsilon_1\\ \varepsilon_2\\ \varepsilon_3\end{Bmatrix} \\ &= \frac{1}{2}\ \varepsilon^{\ T} \quad a \quad f \quad a \quad \varepsilon \end{aligned} \tag{5}$$

If we assume the foam as an idealized homogeneous medium, then the above strain energy can be expressed in terms of the elastic constants, strains and the volume of the cuboid as

$$U = U_0 V = \frac{1}{2} V[\varepsilon]^T[C][\varepsilon] \tag{6}$$

Where U_0 is the strain energy density, V is the volume of the RVE and the $[C]$ is the 3×3 matrix of elastic constants that relate the normal stresses and strains (see Eq. (1)). If the relations in Eqs. (5) and (6) should be valid for any arbitrary set of strains, then the elasticity matrix $[C]$ should be related to $[f]$ as

$$[C] = \frac{1}{V}\ a \quad f \quad a \tag{7}$$

For the case of shear, the calculations can be simplified, as there is no coupling between shear deformation and the normal deformation, and also between shear deformations in different planes. The straightforward method of determining the shear modulus G_{ij} will be to relate the strain energy in the RVE to the strain energy density due to shear:

$$U = \frac{1}{2} G_{ij} \gamma_{ij}^2 V \text{ or } G_{ij} = \frac{2U}{\gamma_{ij}^2 V} \tag{8}$$

V. Results and Discussion

Results obtained for the properties of the equisided tetrakaidecahedron and elongated tetrakaidecahedron unit cell are shown in Table 6 and Table 7 respectively. The results for E and ν match very well with the available analytical models[10]. The deformed and un-deformed configurations of the unit cell for various macro-strains are shown in Figures 12a through Figures 12d. In addition, some parametric studies have been presented in Figure 14a to Figure 14c for equisided and Figure 15a to Figure 15b for elongated respectively.

It is interesting to note that with the equisided tetrakaidecahedron as the unit cell, the results for the properties using either 2-node cubic elements or 3-node quadratic elements do not change much (0.24% difference). This is because of the assumed beam aspect ratio (L/d = 17, see Figure 3, Table 1). With the beams being slender, the classical beam theory assumption holds good and the shear deformation is negligible. Hence Euler-Bernoulli and the Timoshenko beams give pretty much comparable results.

However in the case of the elongated tetrakaidecahedron wherein the beams are short and thick, especially on the squares on the top and the bottom faces (aspect ratio= 2, see: Figure 6, Table 3), the values for the properties have significant difference when a 3-node quadratic element is assumed instead of a 2-node cubic element (9 % difference in the stiffness properties).

Figure 15a and Figure 15b show the differences in the values of elastic constants obtained using 2-node cubic elements and the 3-node quadratic elements when the relative density increases. Hence the existing analytical models[10,11] assuming the unit cell edges completely made out of Euler-Bernoulli beams would not be accurate and bringing in the effect of shear deformation in the analytical formulation would be important.

VI. Conclusions

Finite element based micromechanics has been used to calculate the elastic properties of foams with tetrakaidechedronal unit cells. The results for elastic constants match well with that from available analytical models. It is evident that using finite element methods gives a flexibility to choose between Euler-Bernoulli formulation or the shear-deformable formulation or a mix of both in the same unit cell over the existing analytical models. The biggest advantage of using finite element methods is that any kind of a unit cell with unequal sides that might be obtained from microstructural measurements could be modeled with ease and the technique for computing properties would still remain the same. It would also be easy to extend the same finite element methods to calculate plastic properties for the foam. The same finite element micromechanics methods could also be easily used in the unit cell model to generate multi-axial failure envelopes for foams.

Acknowledgments

This research was supported by a State of Florida Space Research Initiative (SRI) grant awarded to the University of Florida and University of Central Florida. The authors would also like to acknowledge support from the Florida Space Grants Consortium (FSGC).

References

[1]Gibson, L. J., and Ashby, M. F., 1997. *Cellular Solids: structure and properties*. 1st edition, Cambridge university press, U.K,

[2]Thompson, W., 1887. "On the division of space with minimum partitional area." *Philosophical Magazine* 24**,** 503.

[3]Hall, R. B., and Hager, J. W., 1996. "Performance limits for stiffness-critical graphitic foam structures, Comparisons with high-modulus foams, refractory alloys and graphite-epoxy composites". *Journal of Composite Materials* 30

[4]Li, K., Gao, X. L., and Roy, A. K., 2003. "Micromechanics model for three-dimensional open-cell foams using a tetrakaidecahedral unit cell and Castigliano's second theorem.", *Composites Science and Technology* 63**,** 1769-1781.

[5]Arakere, N.K., Knudsen, E., Wells, D., McGill, P., Swanson, G., 2008 "Determination of mixed-mode stress intensity factors, fracture toughness, and crack turning angle for anisotropic foam material", *International Journal of Solids and Structures*, 45, pp. 4936-4951

[6]Karkkainen, R., Sankar, B.V., 2006, "A direct micromechanics method for analysis of failure initiation of plain weave textile composites", *Composite Science and Technology* 66, 137-150

[7]Sankar, BV, Marrey, RV., 1997. "Analytical Method for Micromechanics of Textile Composites", *Composites Science and Technology* 57: 703 – 713.
[8]Choi, S., Sankar, BV., 2005, "A micromechanical method to predict the fracture toughness of cellular materials", *International Journal of Solids and Structures* 42: 1797-1817
[9]Lee, SJ., Wang, J., Sankar, BV., 2007, "Fracture toughness of foams with tetrakaidecahedral unit cells", *International Journal of Solids and Structures* 44 : 4053- 4067
[10]Sullivan, R.M., Ghosn, L.J., Lerch, B.J, 2008, "Application of an Elongated Kelvin Model to Space Shuttle Foams", *AIAA* 2008-1786
[11]Sullivan, R.M., Ghosn, L.J., Lerch, B.J, 2007, "A general tetrakaidecahedron model for open-celled foams", *International Journal of Solids and Structures* 45: 1754-1765
[12]Wright L.S. and Lerch B.A., 2005, "Characterization of space shuttle insulative materials", *NASA/TM-2005-213596*
[13]Huber A.T., Gibson, L.J., 1988, "Anisotropy of foams", *Journal of Material Science*, 1988, Vol. 23, pp.3031-3040
[14]Zhu, H.X., Knott, J.F., Mills, N.J., 1997, "Analysis of the Elastic Properties of Open-Cell Foams with Tetrakaidecahedral Cells", *Journal of Mechanics and Physics of Solids*, Vol.45, No.3, pp. 319-343
[15]Weisstein, E. W., "Truncated Octahedron, MathWorld--A Wolfram Web Resource": http://mathworld.wolfram.com/TruncatedOctahedron.html

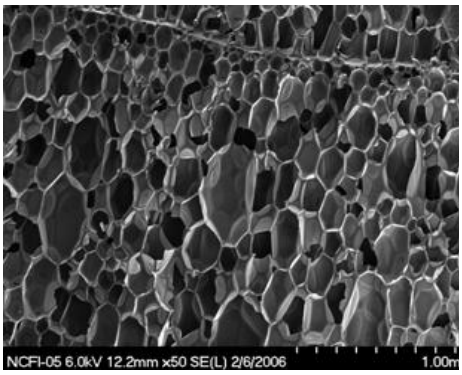

Figure 1: NCFI24-124 (Ref 10)

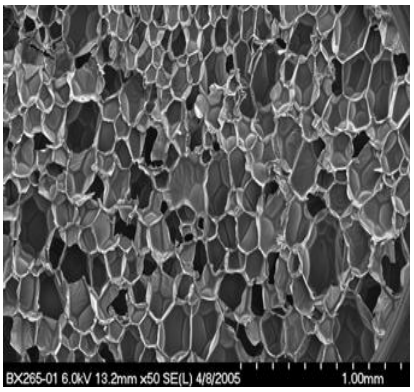

Figure 2. BX265 (Ref 10)

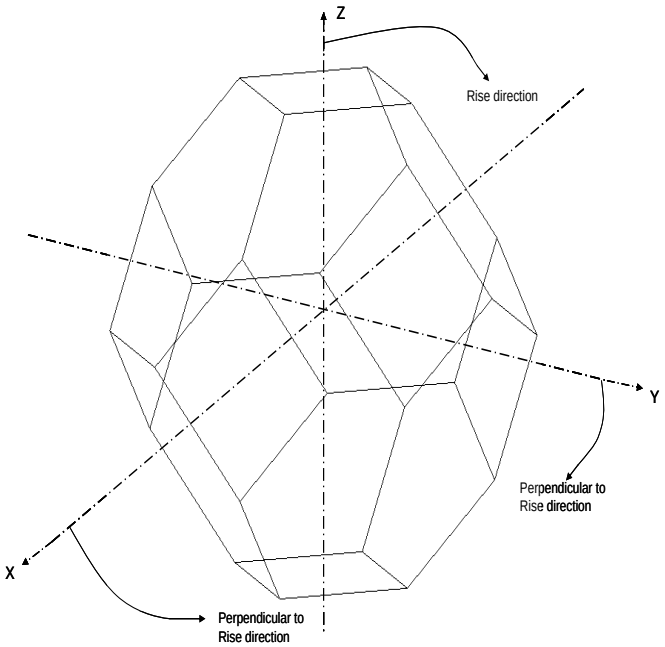

Figure 3. Elongated Tetrakaidecahedron

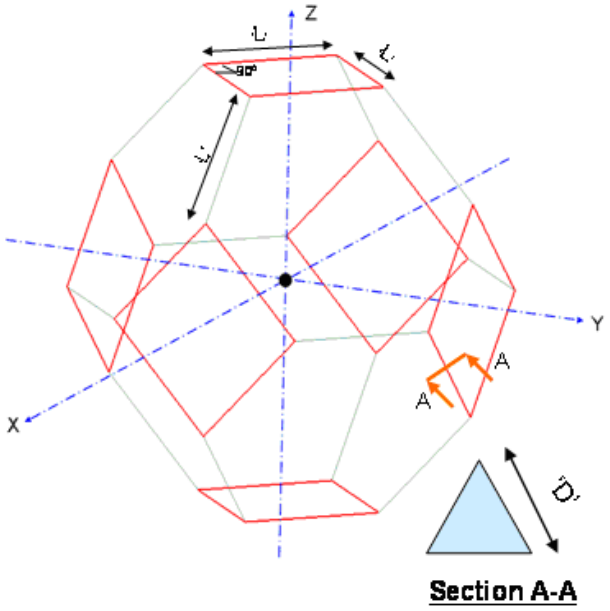

Figure 4. Equi-sided Tetrakaidecahedron

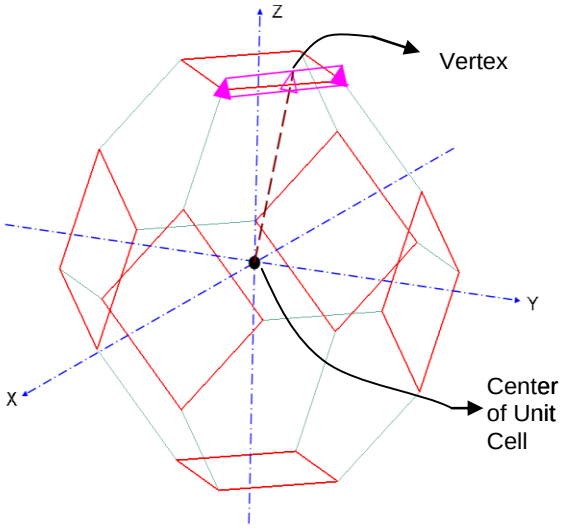

Figure 5. Orientation of the cross section

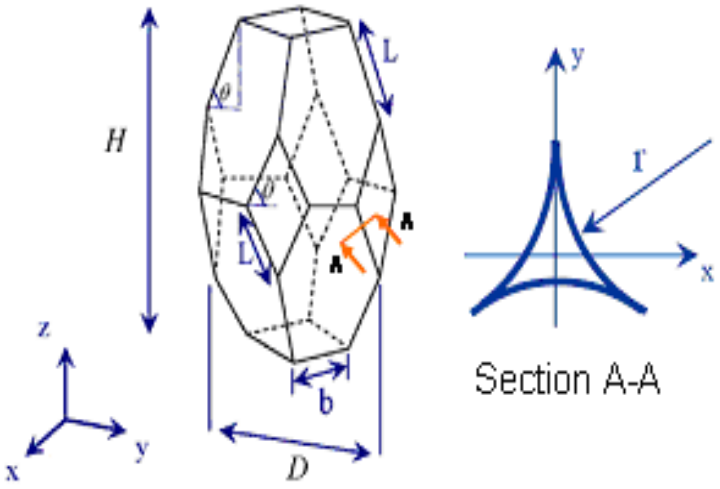

Figure 6. Elongated Tetrakaidecahedron (Ref 11)

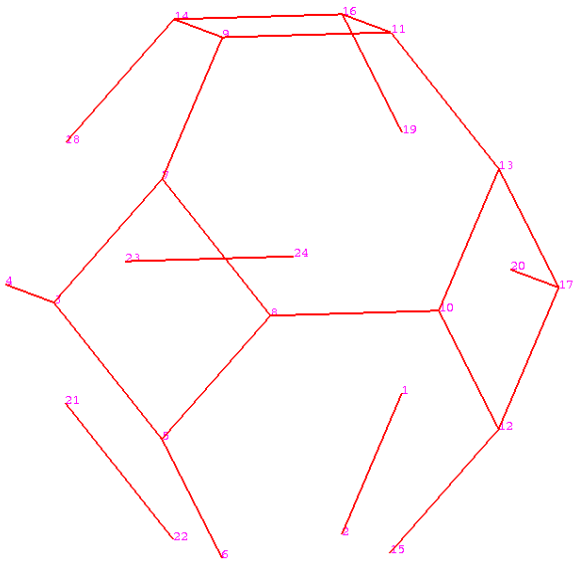

Figure 7. Meshed beam model of a Tetrakaidecahedron unit cell

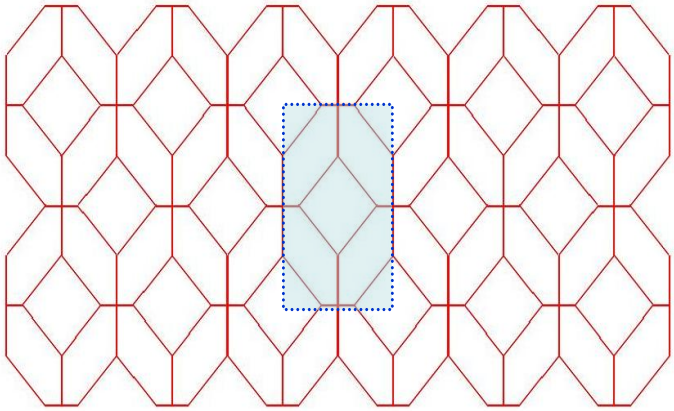

Figure 8. Representative volume element

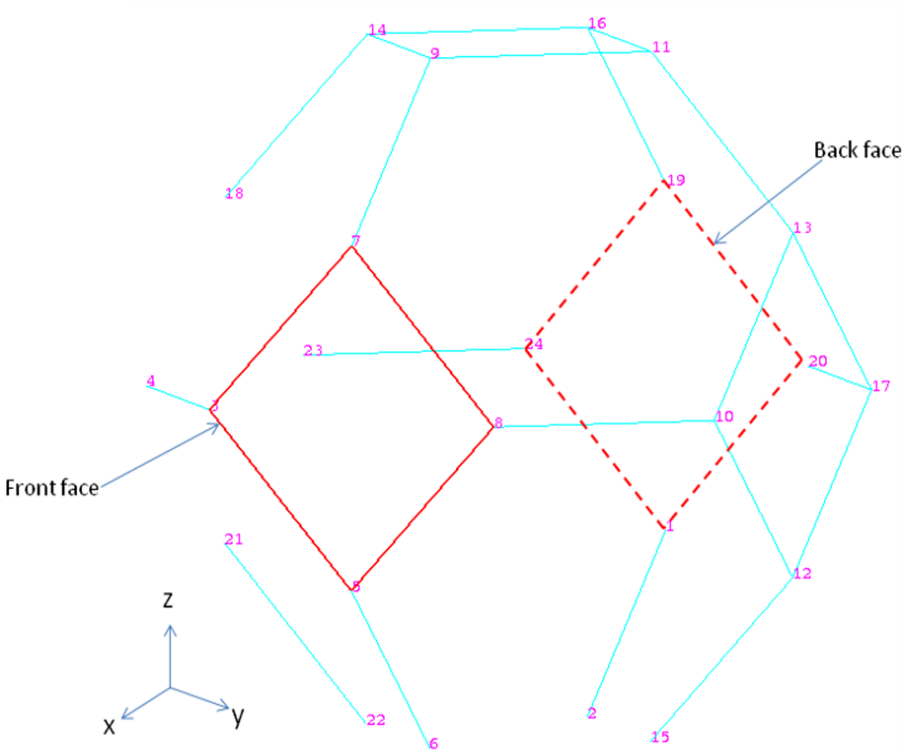

Figure 9. Nodes subjected to Periodic boundary conditions in the X-direction

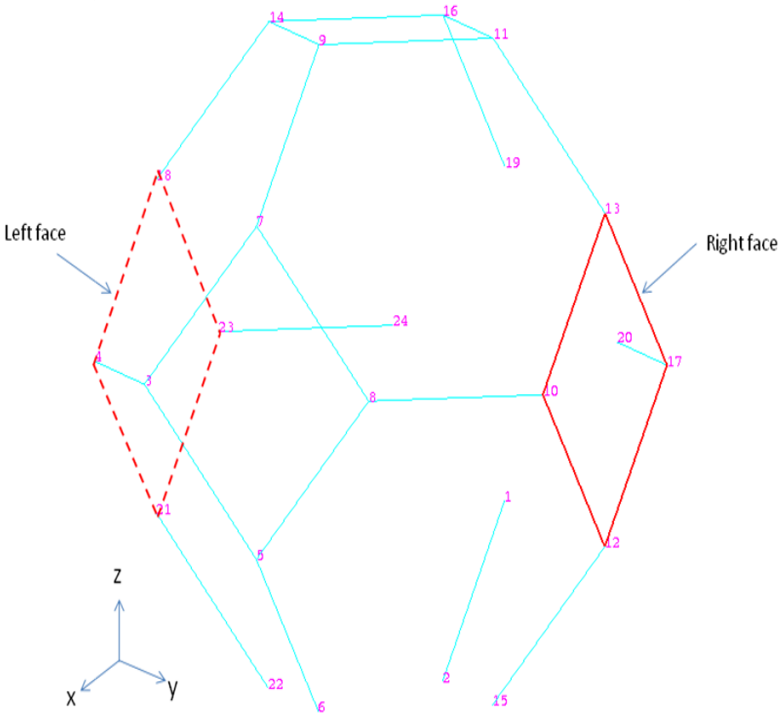

Figure 10. Nodes subjected to Periodic boundary conditions in the Y-direction

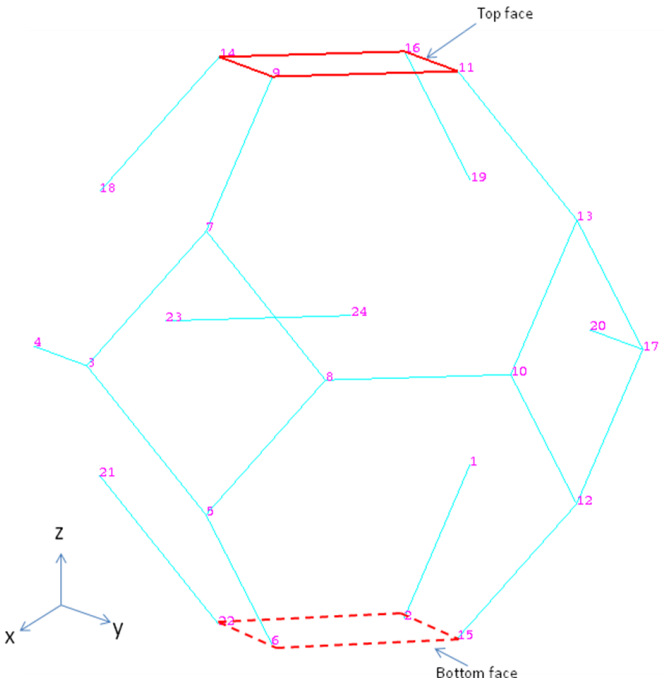

Figure 11. Nodes subjected to Periodic boundary conditions in the Z-direction

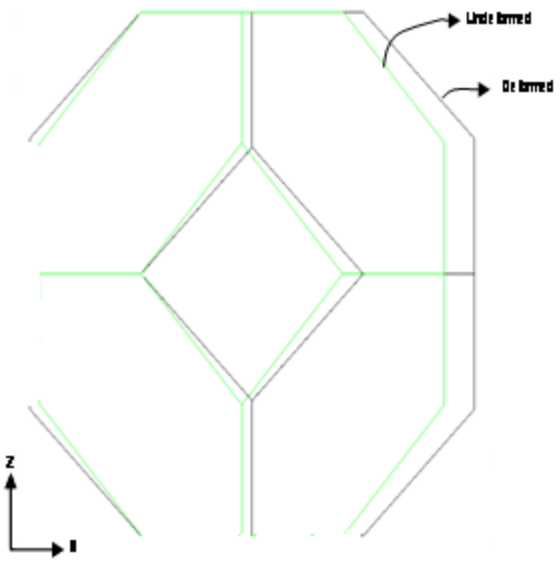

Figure 12a. Equisided tetrakaidecahedron subjected to $\varepsilon_x = 0.01$

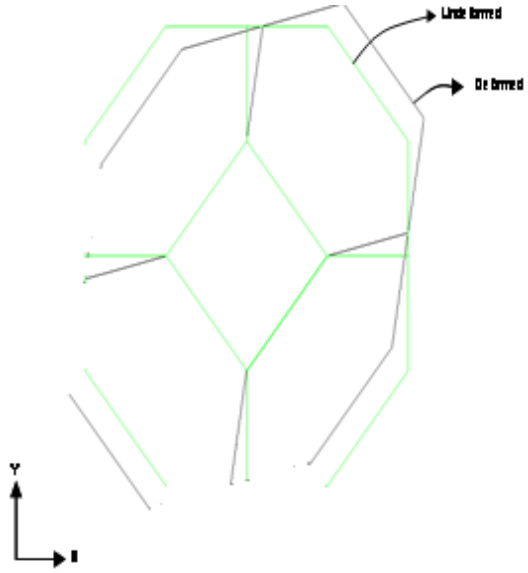

Figure 12b. Equisided tetrakaidecahedron subjected to $\gamma_{xy} = 0.01$

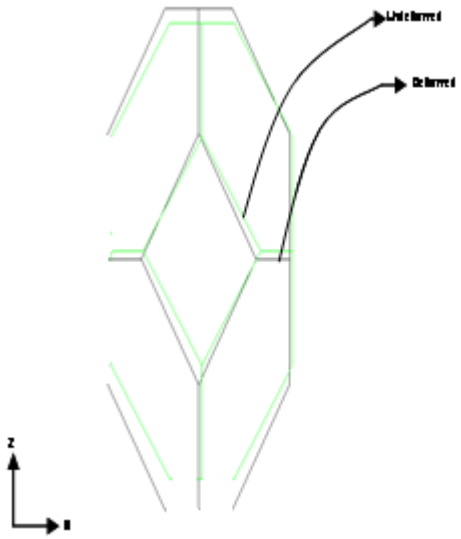

Figure 12c. Elongated tetrakaidecahedron subjected to $\varepsilon_z = 0.01$

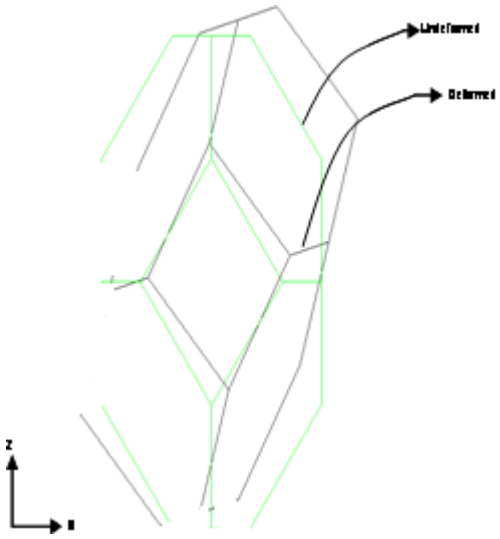

Figure 12d. Elongated tetrakaidecahedron subjected to $\gamma_{xz} = 0.01$

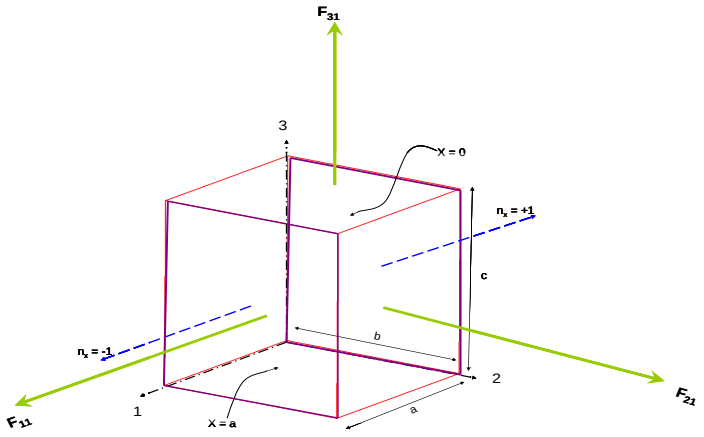

Figure 13. Forces F_{11}, F_{11}, F_{31} when the RVE is deformed in the 1-direction

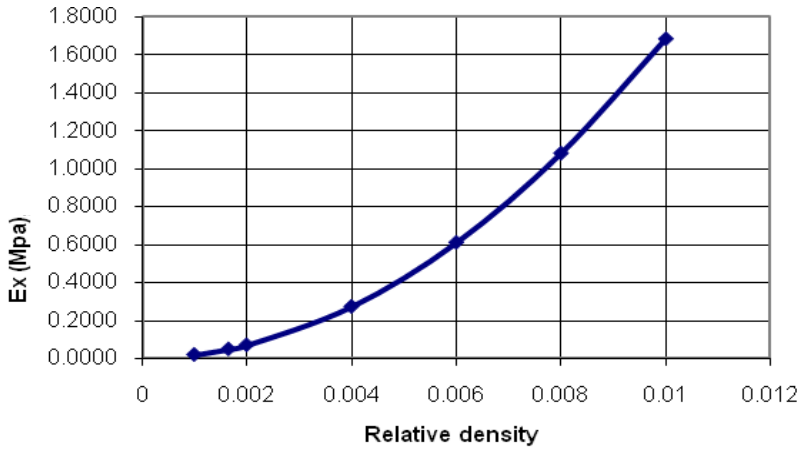

Figure 14a. Graph showing trends of properties for Equisided Unit cell modeled with 2 node cubic elements

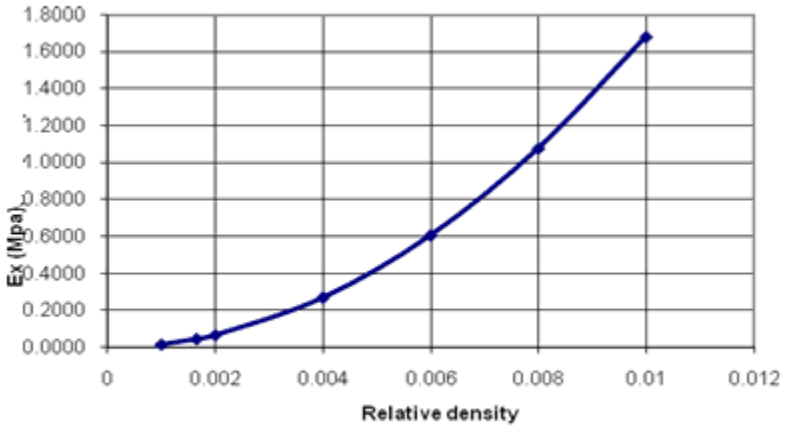

Figure 14b. Graph showing trends of properties for Equisided Unit cell modeled with 3 node quadratic elements

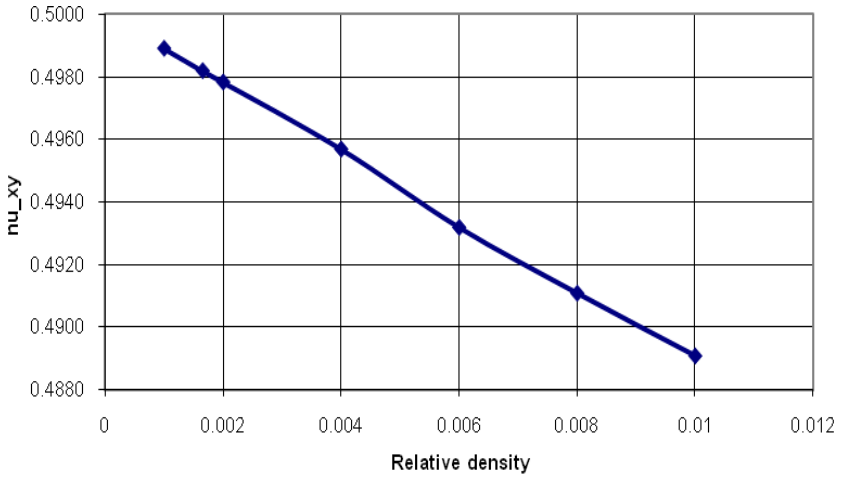

Figure 14c. Graph showing trends of properties for Equisided Unit cell modeled with 3 node quadratic elements

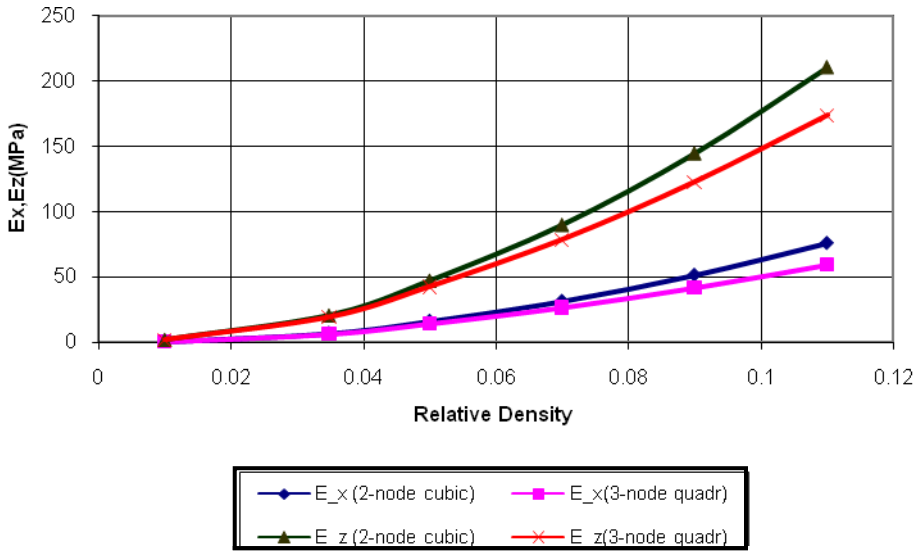

Figure 15a. Graph showing trends of properties for Elongated Unit cell

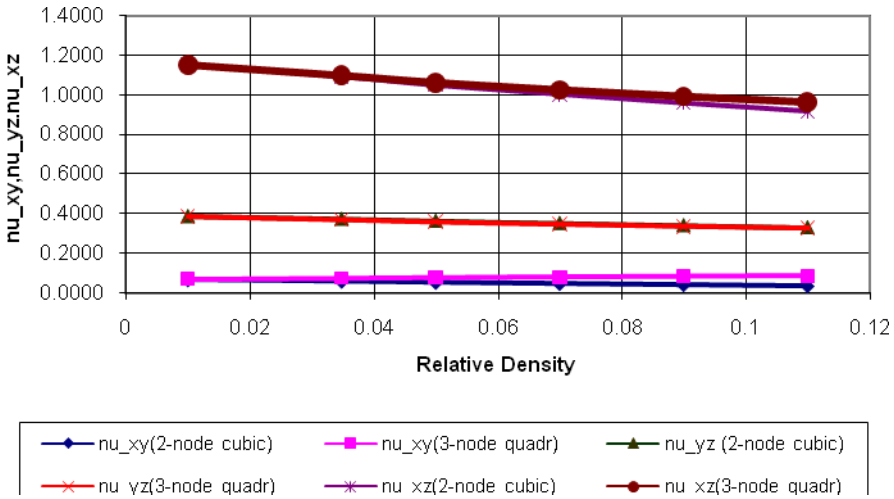

Figure 15b. Graph showing trends of properties for Elongated Unit cell

Table 1: Properties of the Strut material used in the example – Equisided tetrakaidecahedron

Density, ρ_s (Kg/m^3)	Elastic modulus, E_s (GPa)	Poisson ratio, v_s
1650	23.42	0.33

Dimensions used for the Equisided Tetrakaidecahedron (Figure 3)

L (mm)	D (mm)	Relative density
1	0.06	0.001653

Table 2: Cross Section Properties – Equisided tetrakaidecahedron

	Independent edges
Cross sectional area, A (m^2)	1.5588×10^{-9}
Moment of Inertia, I_x ,I_y (m^4)	2.3382×10^{-19}
Polar moment of Inertia, J (m^4)	4.6765×10^{-19}

Table 3: Properties of the Strut material used in the example – Elongated tetrakaidecahedron

Density, ρ_s (Kg/m^3)	Elastic modulus, E_s (GPa)	Poisson ratio, v_s
1650	17	0.33

Dimensions used for the Elongated Tetrakaidecahedron (Figure 7)

l (μm)	b (μm)		θ (degrees)
77.2	35.6		53.57
r (μm)	H (μm)	D (μm)	Relative density
26	248.85	142.04	0.03481

Table 4: Cross Section Properties – Elongated tetrakaidecahedron

	Independent edges
Cross sectional area, A (m^2)	1.024×10^{-10}
Moment of Inertia, I_x ,I_y (m^4)	1.403×10^{-21}
Polar moment of Inertia, J (m^4)	2.806×10^{-21}

Table 5a: Periodic Boundary conditions - Unit strain applied in Principal X direction

Faces	Pair of node numbers	Difference in displacements between the pairs of nodes					
		ΔU_x	ΔU_y	ΔU_z	$\Delta \theta_x$	$\Delta \theta_y$	$\Delta \theta_z$
Top – Bottom (Faces normal to the principal Z-axis)	16 - 2	0	0	0	0	0	0
	14 - 22	0	0	0	0	0	0
	9 - 6	0	0	0	0	0	0
	11 - 15	0	0	0	0	0	0
Front – Back (Faces normal to the principal X-axis)	7 - 19	a_1	0	0	0	0	0
	3 - 24	a_1	0	0	0	0	0
	5 - 1	a_1	0	0	0	0	0
	8 - 20	a_1	0	0	0	0	0
Left – Right (Faces normal to the principal Y-axis)	18 - 13	0	0	0	0	0	0
	4 - 10	0	0	0	0	0	0
	21 - 12	0	0	0	0	0	0
	23 - 17	0	0	0	0	0	0

Table 5b: Periodic Boundary conditions - Unit strain applied in Principal Y direction

Faces	Pair of node numbers	Difference in displacements between the pairs of nodes					
		ΔU_x	ΔU_y	ΔU_z	$\Delta \theta_x$	$\Delta \theta_y$	$\Delta \theta_z$
Top – Bottom (Faces normal to the principal Z-axis)	16 - 2	0	0	0	0	0	0
	14 - 22	0	0	0	0	0	0
	9 - 6	0	0	0	0	0	0
	11 - 15	0	0	0	0	0	0
Front – Back (Faces normal to the principal X-axis)	7 - 19	0	0	0	0	0	0
	3 - 24	0	0	0	0	0	0
	5 - 1	0	0	0	0	0	0
	8 - 20	0	0	0	0	0	0
Left – Right (Faces normal to the principal Y-axis)	18 - 13	0	a_2	0	0	0	0
	4 - 10	0	a_2	0	0	0	0
	21 - 12	0	a_2	0	0	0	0
	23 - 17	0	a_2	0	0	0	0

Table 5c: Periodic Boundary conditions - Unit strain applied in Principal Z direction

Faces	Pair of node numbers	Difference in displacements between the pairs of nodes					
		ΔU_x	ΔU_y	ΔU_z	$\Delta \theta_x$	$\Delta \theta_y$	$\Delta \theta_z$
Top – Bottom (Faces normal to the principal Z-axis)	16 - 2	0	0	a_3	0	0	0
	14 - 22	0	0	a_3	0	0	0
	9 - 6	0	0	a_3	0	0	0
	11 - 15	0	0	a_3	0	0	0
Front – Back (Faces normal to the principal X-axis)	7 - 19	0	0	0	0	0	0
	3 - 24	0	0	0	0	0	0
	5 - 1	0	0	0	0	0	0
	8 - 20	0	0	0	0	0	0
Left – Right (Faces normal to the principal Y-axis)	18 - 13	0	0	0	0	0	0
	4 - 10	0	0	0	0	0	0
	21 - 12	0	0	0	0	0	0
	23 - 17	0	0	0	0	0	0

Table 5d: Periodic Boundary conditions - Unit shear strain $\gamma_{xy} = 1$

Faces	Pair of node numbers	Difference in displacements between the pairs of nodes					
		ΔU_x	ΔU_y	ΔU_z	$\Delta \theta_x$	$\Delta \theta_y$	$\Delta \theta_z$
Top – Bottom (Faces normal to the principal Z-axis)	16 - 2	0	0	0	0	0	0
	14 - 22	0	0	0	0	0	0
	9 - 6	0	0	0	0	0	0
	11 - 15	0	0	0	0	0	0
Front – Back (Faces normal to the principal X-axis)	7 - 19	0	$a_1/2$	0	0	0	0
	3 - 24	0	$a_1/2$	0	0	0	0
	5 - 1	0	$a_1/2$	0	0	0	0
	8 - 20	0	$a_1/2$	0	0	0	0
Left – Right (Faces normal to the principal Y-axis)	18 - 13	$a_2/2$	0	0	0	0	0
	4 - 10	$a_2/2$	0	0	0	0	0
	21 - 12	$a_2/2$	0	0	0	0	0
	23 - 17	$a_2/2$	0	0	0	0	0

Table 5e: Periodic Boundary conditions - Unit shear strain $\gamma_{yz} = 1$

Faces	Pair of node numbers	Difference in displacements between the pairs of nodes					
		ΔU_x	ΔU_y	ΔU_z	$\Delta \theta_x$	$\Delta \theta_y$	$\Delta \theta_z$
Top – Bottom (Faces normal to the principal Z-axis)	16 - 2	0	$a_2/2$	0	0	0	0
	14 - 22	0	$a_2/2$	0	0	0	0
	9 - 6	0	$a_2/2$	0	0	0	0
	11 - 15	0	$a_2/2$	0	0	0	0
Front – Back (Faces normal to the principal X-axis)	7 - 19	0	0	0	0	0	0
	3 - 24	0	0	0	0	0	0
	5 - 1	0	0	0	0	0	0
	8 - 20	0	0	0	0	0	0
Left – Right (Faces normal to the principal Y-axis)	18 - 13	0	0	$a_3/2$	0	0	0
	4 - 10	0	0	$a_3/2$	0	0	0
	21 - 12	0	0	$a_3/2$	0	0	0
	23 - 17	0	0	$a_3/2$	0	0	0

Table 5f: Periodic Boundary conditions - Unit shear strain $\gamma_{xz} = 1$

Faces	Pair of node numbers	Difference in displacements between the pairs of nodes					
		ΔU_x	ΔU_y	ΔU_z	$\Delta \theta_x$	$\Delta \theta_y$	$\Delta \theta_z$
Top – Bottom (Faces normal to the principal Z-axis)	16 - 2	$a_1/2$	0	0	0	0	0
	14 - 22	$a_1/2$	0	0	0	0	0
	9 - 6	$a_1/2$	0	0	0	0	0
	11 - 15	$a_1/2$	0	0	0	0	0
Front – Back (Faces normal to the principal X-axis)	7 - 19	0	0	$a_3/2$	0	0	0
	3 - 24	0	0	$a_3/2$	0	0	0
	5 - 1	0	0	$a_3/2$	0	0	0
	8 - 20	0	0	$a_3/2$	0	0	0
Left – Right (Faces normal to the principal Y-axis)	18 - 13	0	0	0	0	0	0
	4 - 10	0	0	0	0	0	0
	21 - 12	0	0	0	0	0	0
	23 - 17	0	0	0	0	0	0

Table 6: Results for Equi-sided Tetrakaidecahedron

Property	FEM			ANALYTICAL	% DIFFERENCE (FEM & analytical)
	Euler-Bernoulli (2-node cubic)	Shear deformable (3-node quadratic)	% difference		
E_x (Gpa)	46.7×10^{-6}	46.6×10^{-6}	0.24	46.4×10^{-6}	0.55
E_y (Gpa)	46.7×10^{-6}	46.6×10^{-6}	0.24	46.4×10^{-6}	0.55
E_z (Gpa)	46.7×10^{-6}	46.6×10^{-6}	0.24	46.4×10^{-6}	0.55
v_{xy}	0.498	0.498	0.11	0.497	0.14
v_{xz}	0.498	0.498	0.11	0.497	0.14
v_{yx}	0.498	0.498	0.11	0.497	0.14
v_{yz}	0.498	0.498	0.11	0.497	0.14
v_{zx}	0.498	0.498	0.11	0.497	0.14
v_{xy}	0.498	0.498	0.11	0.497	0.14
G_{xy} (Gpa)	14.9×10^{-6}	14.8×10^{-6}	0.43	14.9×10^{-6}	0.35
G_{yz} (Gpa)	14.9×10^{-6}	14.8×10^{-6}	0.43	14.9×10^{-6}	0.35
G_{xz} (Gpa)	14.9×10^{-6}	14.8×10^{-6}	0.43	14.9×10^{-6}	0.35

Table 7: Results for Elongated Tetrakaidecahedron

Property	FEM			ANALYTICAL	% DIFFERENCE (FEM & analytical)
	Euler-Bernoulli (2-node cubic)	Shear deformable (3-node quadratic)	% difference		
E_x (Mpa)	7.09	6.50	-9.04%	7.07	0.29
E_y (Mpa)	7.09	6.50	-9.04%	7.07	0.29
E_z (Mpa)	20.63	19.28	-6.99%	20.8	-0.82
v_{xy}	0.0588	0.0757	22.28%	0.0598	-1.84
v_{xz}	0.3745	0.3694	-1.39%	0.373	0.47
v_{yx}	0.0588	0.0757	22.28%	0.0599	-1.84
v_{yz}	0.3745	0.3694	-1.39%	0.373	0.47
v_{zx}	1.0934	1.0991	0.52%	1.09	-0.31
v_{xy}	1.0934	1.0991	0.52%	1.09	-0.31
G_{xy} (Mpa)	2.07	1.95	-6.03%		
G_{yz} (Mpa)	6.74	6.25	-7.88%		
G_{xz} (Mpa)	6.74	6.25	-7.88%		